materials

MDPI

Article

Experimental and Numerical Study on Chloride Transport in Unsaturated Concrete: Highlighting Temperature, Humidity, and Mineral Admixtures

Zhantao Du [1,2], Zuquan Jin [1,2,*], Shicai Li [1,2,*], Huan Xue [1,3] and Rui Zhao [1]

[1] School of Civil Engineering, Qingdao University of Technology, Qingdao 266520, China; duzhantao1101@163.com (Z.D.)
[2] Engineering Research Center of Concrete Technology under Marine Environment, Ministry of Education, Qingdao 266520, China
[3] Qingdao Branch of Beijing Zhongchang Engineering Consulting Co., Ltd., Qingdao 266520, China
* Correspondence: jinzuquan@126.com (Z.J.); lishicai1995@163.com (S.L.)

Abstract: Chloride transport within concrete is critical for the durability of reinforced concrete structures; however, its diffusion under the coupling action of temperature and humidity has not been fully comprehended. Therefore, in this work, the coupling effects of temperature, relative humidity, and mineral admixtures on chloride transport in concrete were investigated through experimental and numerical simulation work. The results show that the chloride diffusion coefficient decreases with the decreased temperature and growth of relative humidity; however, the chloride concentration on the concrete surface is increased with the growth of temperature and relative humidity. Moreover, compounding about 15% fly ash (FA) and 30% granulated ground blast furnace slag (GGBS) to replace the cement is the most beneficial for improving the antichloride capacity of concrete, considering also the strength. In addition, the numerical simulation considering the coupled effect of temperature and relative humidity of chloride transport in concrete has good agreement with that of experimental results.

Keywords: unsaturated concrete; chloride transport; diffusion coefficient; numerical simulation; mineral admixtures; temperature–humidity coupling

check for updates

Citation: Du, Z.; Jin, Z.; Li, S.; Xue, H.; Zhao, R. Experimental and Numerical Study on Chloride Transport in Unsaturated Concrete: Highlighting Temperature, Humidity, and Mineral Admixtures. *Materials* **2024**, *17*, 930. https://doi.org/10.3390/ma17040930

Academic Editors: Dario De Domenico and Carlos Leiva

Received: 21 January 2024
Revised: 11 February 2024
Accepted: 15 February 2024
Published: 17 February 2024

Copyright: © 2024 by the authors. Licensee MDPI, Basel, Switzerland. This article is an open access article distributed under the terms and conditions of the Creative Commons Attribution (CC BY) license (https://creativecommons.org/licenses/by/4.0/).

1. Introduction

Chloride ion is a sensitive keyword when considering the durability performance of reinforced concrete structures, especially under harsh marine environments [1–3]. In chloride-rich circumstances, reinforced bars embedded in concrete cover will corrode under the conditions of moisture and oxygen due to the serious damage to the rebars' electrochemical stability [4,5]. Furthermore, rebar corrosion inside concrete will trigger a series of fatal consequences in the field of civil engineering, which includes the degradation of mechanical properties, load-bearing capacity, and seismic performance of concrete structures. Moisture is not only necessary for cement hydration but is also closely related to the durability of concrete, which plays a role as a carrier for the corrosive media to enter the concrete [6,7]. The moisture variation in concrete is triggered by the water exchange with the external environment. For concrete with a high water–cement ratio, due to its poor compactness, its internal humidity is greatly affected by the environment, and the self-drying effect is not obvious [8,9]. Furthermore, the pore saturation of concrete is determined by the relative humidity; meanwhile, the temperature is considered to influence the diffusion processes. The water transport in concrete not only significantly affects the hardening of concrete but also changes the mass and volume [10,11]. In addition, when the internal relative humidity is higher than the ambient relative humidity, the moisture will be diffused into the air from the concrete inside, resulting in different degrees of dry shrinkage

and tensile stress on the surface of the concrete structures, which seriously impacts the service life and durability performance of reinforced concrete structure [12]. Hence, it is of great concern to reveal the principle of chloride ions' penetration through the concrete cover while evaluating the residual service life of concrete structures [13,14].

Recently, several researchers have conducted extensive studies and attempted to reveal the diffusion process of chloride within concrete using laboratory characterization and numerical simulation [15–18]. Wu et al. [19] presented a study on the durability testing of a concrete facility located within the North Bay Port region and in service for 200 months. They proposed that the apparent chloride diffusion coefficient (D_{app}) and the apparent surface chloride concentration (C_s) follow the log-normal distribution, while m follows a normal distribution. Yu et al. [20] proposed the chloride diffusion coefficient model coupled with environmental factors to describe chloride ingress into concrete with field tests and artificially simulated environment experiments. Wang et al. [21] investigated chloride ion transport in concrete, considering the effect of a dry-exposure ratio under a diurnal tidal environment, and established a time-dependent model of chloride ion transport in concrete considering the effect of dry-exposure ratio. Al-Sodani et al. [22] investigated the correlation between short-term chloride ion migration coefficients and long-term Dapp in concrete with indoor experiments and field exposure experiments. They established a correlation model between field and laboratory results based on the experimental data. Pansera et al. [23] proposed an empirical chloride transport model contemplating the convection–diffusion zones through two Gaussian–Lorentzian functions using nonlinear regression in chloride profiles obtained from field structures located in different marine aggressive zones exposed to the marine environment for more than 40 years.

Lately, much mesoscopic research into chloride transport in concrete has been reported [24–28]. These works concentrate on two aspects: (1) investigating the impact of concrete's mesoscopic phases on chloride transport and (2) developing the equivalent methods from the mesoscale to the macroscale. Lee et al. [29] proposed a coupled transport model considering moisture and chloride distribution in concrete to investigate the influence of a cyclic exposure condition on chloride penetration. Jain et al. [30] developed a numerical model to study the coupled transport of chloride with heat, relative humidity, and oxygen into the concrete. Liu et al. [31] established a modified chloride ion diffusion–convection model for concrete considering curing age, initial water saturation, and the combined effects of chloride ions. These studies have revealed some intrinsic mechanisms of chloride transport in concrete and have demonstrated that mesoscopic research is an effective and reliable method for chloride transport in concrete. However, these investigations did not adequately account for the coupling effects of temperature, relative humidity, and mineral admixtures.

Recently, the authors also conducted relevant studies on this issue, especially in practical marine environments. Despite enormous studies on the point of chloride transportation, there are still several drawbacks to revealing the chloride transport law influenced by other impact factors, such as temperature and relative humidity. Furthermore, a gap still exists in revealing the mechanism of chloride ion transport impacted by external factors. Thus, the chloride ion profile at the concrete cover will be discussed in this paper; meanwhile, concrete with mineral admixture was also involved in this study.

2. Experiments

2.1. Materials

Ordinary Portland cement (OPC, P·O 52.5), granulated ground blast furnace slag (GGBS, S95), and fly ash (FA, Class I) are used as main cementitious materials. Their chemical compositions are shown in Table 1. Crushed granite with a size of 5–20 mm from Lei Xin Group Company (Qingdao, China) is used as coarse aggregate. River sand with a fineness modulus of 2.6 from Qingjian New Material Company (Qingdao, China) is used as fine aggregate. Polycarboxylic acid superplasticizer (JM-PCA) is used to adjust the

workability of fresh concrete. In addition, an air-entraining agent is used to control the air content of fresh concrete by 3–5%.

Table 1. Chemical compositions of binder materials (wt.%).

Constituent	SiO_2	Al_2O_3	Fe_2O_3	CaO	MgO	Na_2O	K_2O	SO_3	P_2O_5
OPC	21.58	4.95	3.29	64.84	3.48	0.56	0.48	0.53	0.12
GGBS	29.05	12.51	1.30	48.34	5.72	0.56	0.08	1.18	0.54
FA	56.90	13.70	4.46	1.90	0.37	0.12	1.55	0.12	0.11

2.2. Experimental Methods

2.2.1. Sample Preparation

The water–binder ratio of concrete was controlled to 0.35. Cubic concrete with the dimensions of 100 mm × 100 mm × 100 mm was prepared as the mix proportion listed in Table 2. Each sample of three is a group and takes the average value as the experimental result. The prepared concrete was cured for 3 d, 7 d, 28 d, 56 d, and 120 d in a standard room with a temperature of 20 ± 2 °C and relative humidity of 95%.

Table 2. Mix proportions of concrete (kg/m^3).

NO.	Cement	GGBS	FA	Sand	Aggregate	Water	Superplasticizer	Air-Entraining Agent
L50	470	–	–	760	1090	165	8	0.19
L51	399.5	–	70.5	760	1090	165	8	0.25
L52	329	–	141	760	1090	165	8	0.25
L53	235	–	235	760	1090	165	8	0.25
F51	399.5	70.5	–	760	1090	165	8	0.12
F52	329	141	–	760	1090	165	8	0.12
F53	235	235	–	760	1090	165	8	0.12
F54	165	305	–	760	1090	165	8	0.12
LF50	240	150	80	760	1090	165	8	0.25

2.2.2. Sensors Arrangement and Monitoring

The sensors (temperature and humidity sensor and thermocouples) and their acquisition instruments used in this study are presented in Figure 1a. The sensor of temperature and humidity (SZWS-SHT15) is produced by Sanzhi Electronic Technology Co., Ltd. (Changsha, China), and its parameters are as follows: Capacitive, the measured temperature range is 0–120 °C (±0.5 °C), and the measured humidity range is 0–100% (±3%). The thermocouple is K-type and its acquisition instrument (34970A) is produced by Agilent Technology Co., Ltd. (Santa Clara, CA, USA).

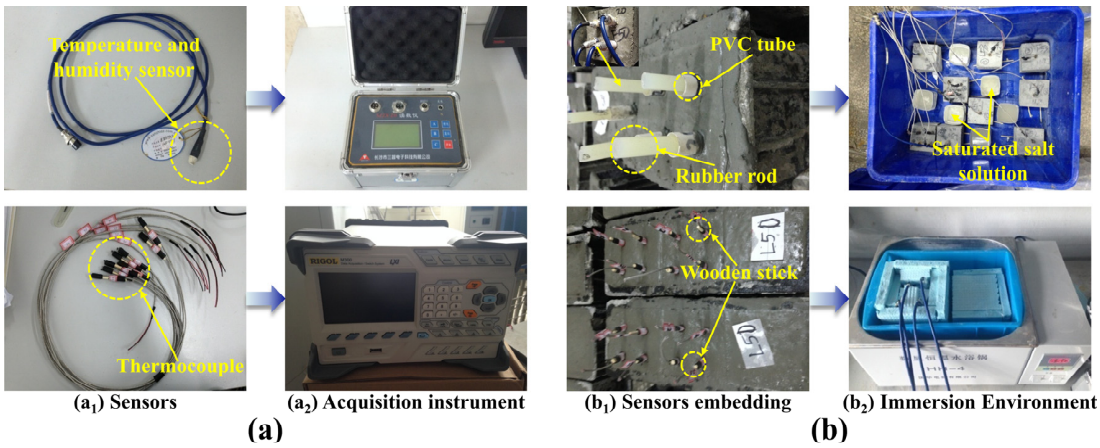

Figure 1. Sensors arrangement and monitoring: (**a**) sensors and their acquisition instrument and (**b**) sensors embedding and immersion environment construction.

The thermocouple was first preprocessed by tying a wooden stick to the bottom of the thermocouple probe to ensure that it could be fixed vertically inside the concrete. After that, a PVC pipe with an inner diameter of 15 mm was inserted into the concrete to a certain depth when pouring into concrete. To prevent the mortar from flowing into the pipe, we placed a rubber rod slightly smaller than the inner diameter of the PVC pipe in advance; after the concrete was finally hardened, the rubber rod was pulled out and replaced by the sensors, as shown in Figure 1b$_1$. In this study, four different humidity spaces were constructed as follows: the concrete specimens were immersed in the water to make it fully saturated and reach 100%, as shown in Figure 1b$_2$. Then, several specimens were removed in a constant temperature and humidity laboratory with a relative humidity of 80% and a temperature of 20 °C to make the humidity reach 80%. After that, they were dried using a drying oven until the humidity reached 65% and saturated the LiBr solution to make it 45%, respectively. Four temperature conditions of 45%, 65%, 80%, and 100% were constructed, respectively, in four different temperatures (5 °C, 25 °C, 45 °C, and 65 °C); after the salt absorption test, the concrete specimens were cleaned on the surface and then grounded using a type DRB-H1 concrete grinder. Furthermore, the content of chloride ions in powder was evaluated using the electrode method according to the Chinese Testing Code of Concrete for Port and Water Engineering, while saturated potassium sulfate was set as the reference electrode.

3. Numerical Simulation

3.1. Theoretical Models

The transport of chloride ions in concrete is an unsteady process. Based on Fick's second law, the transport equation can be expressed as Equation (1) [32]. Figure 2 shows the schematic diagram of ion diffusion within the concrete. Equation (2) is adopted to describe the chloride diffusion process under constant pore saturation. Equation (3) shows the formula to describe the effect of relative humidity on the chloride ion diffusion coefficient [33,34]. Moreover, the chloride migration coefficient will be impacted by temperature, which is presented in Equation (4) [35,36]. The influence of external environmental conditions on chloride ion transport is not a single effect; meanwhile, the increase in temperature will enhance the molecular kinetic energy, thus improving the transport rate of water molecules and resulting in the growth of water in pore structures. Correspondingly, the increase in relative humidity inside the concrete will affect the transport speed of ions or molecules rate, which has a certain effect on the temperature. Equation (5) introduces the empirical formula of chloride ion transport considering the coupled effect of temperature and humidity, while 10 mm was set as a boundary condition [37].

$$\frac{\partial c}{\partial t} = \nabla(D\nabla \mathrm{C}) \tag{1}$$

$$C_f = C_S\left[1 - erf\left(\frac{x}{2\sqrt{Dt}}\right)\right] \tag{2}$$

where c is the ions, t represents the transport time, x represents the transport distance away from the concrete surface, D is the migration coefficient, n_0 is a constant, erf is the error function, C_s is the surface chloride concentration of concrete, and C_f is the chloride concertation at a certain depth.

$$D = \left[1 + \frac{(1 - H_R)^4}{(1 + H_C)^4}\right]^{-1} \tag{3}$$

$$D = \left[\frac{T}{T_1}\right] e^{q\left[\frac{1}{T} - \frac{1}{T_1}\right]} \tag{4}$$

$$\begin{cases} D = D_1\left[\frac{T}{T_1}\right]e^{q\left[\frac{1}{T}-\frac{1}{T_1}\right]}\cdot\left[1-7.032\left(\frac{T}{T_1}\right)^{-0.033}\times\ln(H_R)\right] (x < 10\text{ mm}) \\ D = D_1\left[\frac{T}{T_1}\right]e^{q\left[\frac{1}{T}-\frac{1}{T_1}\right]}\cdot\left[1+\frac{(1-H_R)^4}{(1+H_C)^4}\right]^{-1} (x \geq 10\text{ mm}) \end{cases} \quad (5)$$

where D is the chloride ion transport coefficient, H_R is the relative humidity inside the concrete, H_C is the critical relative humidity, T_1 is the reference temperature (293 K), T is the calculated temperature, q is the activation constant, D_1 is the chloride ion transport coefficient at temperature T_1.

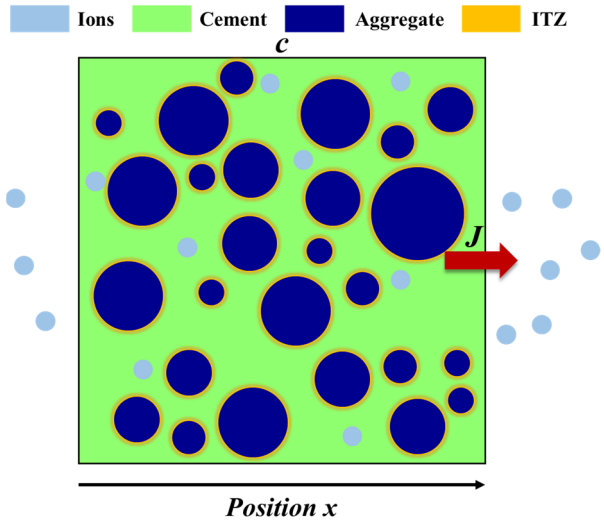

Figure 2. Schematic diagram of ion transport.

3.2. Model Establishment

Based on the theoretical models mentioned above, chloride ion transport was simulated using the software COMSOL Multiphysics (6.1). A two-dimensional model of concrete was established to a cross-section sized 100 mm × 100 mm by randomly distributing circles. The model was divided into three phases: cement paste, fine aggregate, and coarse aggregate. Moreover, the interfacial transitional zone (ITZ) between cement paste and aggregates was modeled with a thickness of 70 μm [38], as shown in Figure 3a. The model was meshed as follows: regular-size triangular meshing for the cement paste, boundary-layer meshing for the interface zone, and finer-size triangular meshing for the aggregates, as shown in Figure 3b. From the physical viewpoint, this model optimizes the aggregate interface and is more in line with the practical situation with a random arrangement of coarse aggregates and fine aggregates. The diffusion coefficient of the ITZ is 4×10^{-10} m^2/s, and that of aggregate is 4×10^{-13} m^2/s. Furthermore, the water–cement ratio (w/c) was set as 0.35, and the concrete density was 2500 kg/m^3. In addition, the surface chloride ion concentration can be calculated as Equation (6). The values of the parameters used in the calculations are shown in Table 3.

$$C_{S,Cl} = A_{S,Cl}\left(\frac{w}{b}\right)r_{C,Cl} \quad (6)$$

where $C_{S,Cl}$ is the surface chloride ion concentration, $A_{S,Cl}$ is the regression coefficient of the surface chloride content, w/b is the water–cement ratio, and $\gamma_{C,Cl}$ is the fractional coefficient of the surface chloride ion concentration.

Table 3. Parameters and values for calculation.

Parameter	Value	Units
D_1	4×10^{-12}	m^2/s
D_2	4×10^{-10}	m^2/s

Table 3. *Cont.*

Parameter	Value	Units
D_3	4×10^{-13}	m^2/s
T_{ref}	293.15	K

Note: D_1, D_2, and D_3 are the chloride diffusion coefficients of the cement paste, ITZ, and aggregate (coarse and fine aggregate), respectively. T_{ref} is the standard temperature. q is the activation constant.

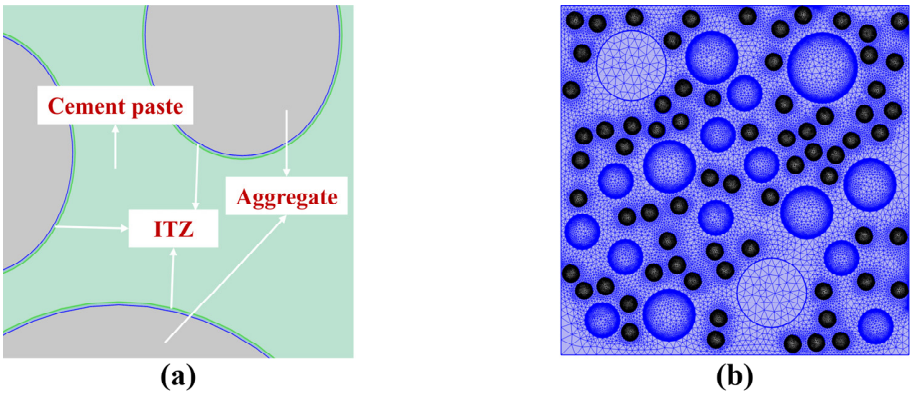

Figure 3. Two-dimensional model of concrete: (**a**) ITZ establishment and (**b**) model meshing.

4. Results and Discussion

4.1. Compressive Strength of Concrete

The compressive strength of concrete was tested after curing for 3 d, 7 d, 28 d, 56 d, and 120 d, as shown in Figure 4. The early compressive strength (–7 d) of OPC-concrete was improved by the replacement of FA with a dosage of 15%, while it was decreased when the dosage reached 30% and 50%, as shown in Figure 4a. However, the compressive strength of all FA concretes was increased by about 32.4% more than OPC concrete when the curing age reached 120 d. Therefore, the early compressive strength of concrete can be decreased due to the excessive addition of FA, while its effect was positive for its long-term compressive strength. As presented in Figure 4b, the compressive strength of OPC concrete after curing for 28 d was improved by about 31.5%, 45.8%, 51.1%, and 49.7% when the dosage of GGBS was 15%, 30%, 50%, and 65%, respectively. The long-term compressive strength was improved as the same trend. Therefore, the compressive strength of concrete can be improved with the increased dosage of GGBS until the dosage exceeds 50%. In addition, there is no significant improvement in the early compressive strength of OPC concrete when simultaneously adding FA and GGBS, as presented in Figure 4c. Meanwhile, compared to the single addition of FA or GGBS, the compressive strength of FA+GGBS concrete was decreased by about 14.6% and 23.3% for the age of 28 d, and 8.4% and 17.4% for the age of 120 d. Therefore, the compressive strength of concrete can be significantly improved by adding 15% FA or 50% GGBS.

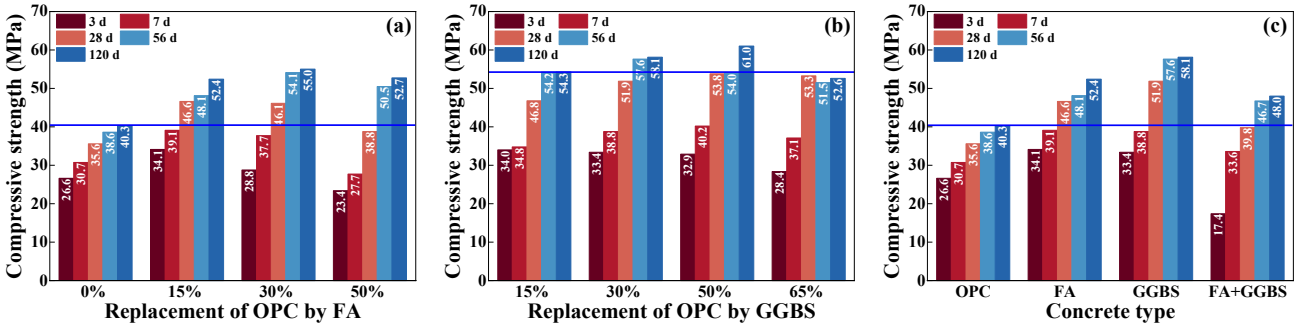

Figure 4. Compressive strength of concrete. (**a**) Effect of FA; (**b**) effect of GGBS; (**c**) effect of compounding FA and GGBS.

4.2. Chloride Transport in Unsaturated Concrete

4.2.1. Effect of Temperature on Chloride Transport

The free chloride concentration of LF50 concrete surface was measured after eroding in the environment with an RH of 65% and four temperatures (5 °C, 25 °C, 45 °C, and 65 °C) for 10 d, as presented in Figure 5. The chloride concentration on the surface area was 0.290% at 5 °C, which tends to be stable at a depth of approximately 5 mm. Similarly, at 25 °C, the chloride concentration at the surface was about 0.275%, and the diffusion depth was about 5 mm. However, the surficial chloride concentration was significantly improved to 0.610% and 2.264% when the temperature reached 45 °C and 65 °C, respectively. Meanwhile, the diffusion depth was also increased to 10 mm. The chloride ion distribution after capillary salt absorption at 65 °C was fitted according to Fick's second law to obtain the diffusion coefficient (D) and chloride concentration (C_s) of the concrete surface, as shown in Figure 5b. The correlation coefficient (R^2) was 0.983, indicating the fitting result was reliable. The confidence band of 95% presented in the figure can also prove that result. In addition, the correlation between the chloride diffusion coefficient and temperature was established according to Arrhenius' empirical formula (Equation (7)), as presented in Figure 5c. The chloride diffusion coefficient of concrete gradually increased with the increased temperature; meanwhile, the migration rate of chloride showed a similar tendency. From a physical point of view, the chloride transport was accelerated when the temperature increased; meanwhile, the concentration was higher due to a faster chloride migration coefficient.

$$\frac{d \ln D}{dT} = \frac{E_a}{RT^2} \tag{7}$$

where the slope is the apparent activation energy E_a (j·mul^{-1}), the intercept is the pre-exponential factor, A, D is the chloride diffusion coefficient (10^{-12} m^2/s), and T is the thermodynamic temperature (K).

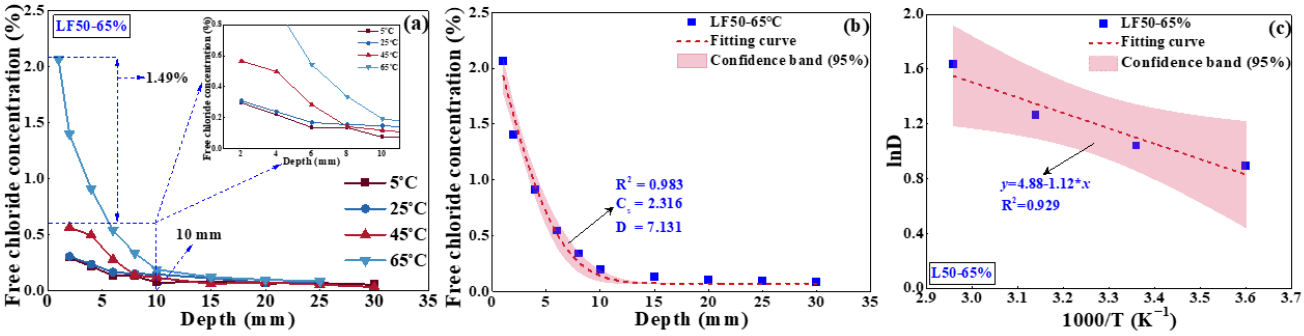

Figure 5. Free chloride concentration of concrete surface: (**a**) effect of temperature, (**b**) fitting curve, and (**c**) regression results between chloride diffusion coefficient and temperature.

4.2.2. Effect of Relative Humidity on Chloride Transport

The free chloride concentration of concrete (L50 and LF50) surface was measured after eroding in an environment with a temperature of 25 °C and four relative humidities (45%, 65%, 80%, and 100%) for 10 d, as presented in Figure 6. Meanwhile, the diffusion coefficient and chloride concentration of the concrete surface obtained by fitting according to Fick's second law. The diffusion coefficient of concrete is decreased with the increased relative humidity. However, the C_s is increased with the growth of relative humidity, especially for LF50 concrete. The C_s of LF50 concrete is increased from 0.229% to 0.467% when the relative humidity is increased from 45% to 100%. On the one hand, the chloride ion diffusion is inhibited by the compound replacement of FA and GGBS, inducing more chlorides to be enriched on the concrete surface. Moreover, chloride diffusion is dependent on moisture transport, while more moisture migrates from the concrete surface to the

interior when the relative humidity of the environment is lower. It can be further observed that the penetration depth of concrete decreases with the increase in internal humidity; the penetration depth of chlorides is about 20 mm, 15 mm, 15 mm, and 10 mm when the relative humidity is 45%, 65%, 80%, and 100%. In addition, it is noted that under unsaturated conditions (not a relative humidity of 100%), there are convection zones that exist on the concrete surface due to capillary adsorption. Therefore, the chloride diffusion will be inhibited by the increased relative humidity; meanwhile, the chloride will be enriched on the concrete surface.

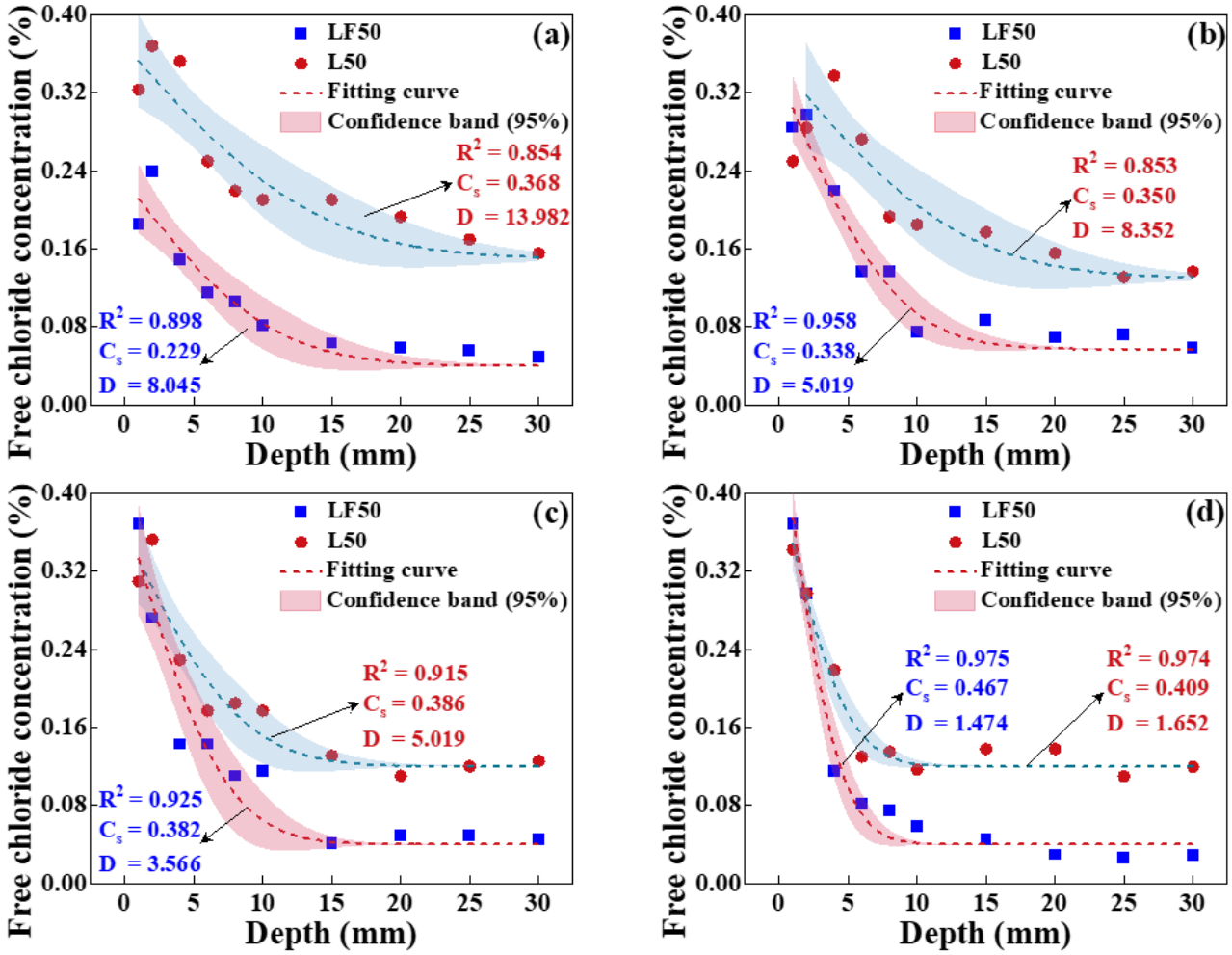

Figure 6. Free chloride concentration of LF50 concrete at the relative humidity of (**a**) 45%, (**b**) 65%, (**c**) 80%, and (**d**) 100%.

Figure 7 shows the fitting result of the chloride diffusion coefficient and relative humidity in concrete. A new function is established, as shown in Equation (8). There is a linear decreasing trend of the chloride diffusion coefficient with the rising of the relative humidity. The main reason for this phenomenon is that the capacity of chloride penetration is stronger when relative humidity is low due to the water absorption ability. Meanwhile, chloride ion concentration will be much higher, accompanied by moisture going inside the concrete. The capillary absorption capacity is weakened and almost zero when the relative humidity reaches 100%.

$$D = a - bR_H \tag{8}$$

where D is the chloride migration coefficient (10^{-12} m^2/s), R_H is the relative internal humidity of concrete, a and b are constant values which depend on the concrete type and temperature.

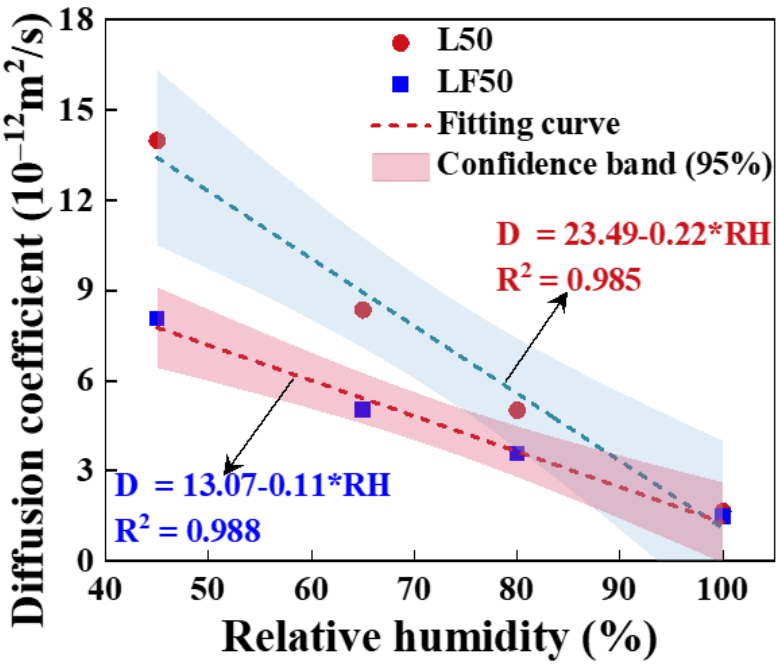

Figure 7. The fitting result of the chloride diffusion coefficient and relative humidity.

4.2.3. Effect of Mineral Admixtures on Chloride Transport

(1) Effect of adding FA on chloride transport

Figure 8 shows the chloride ion concentration of concrete with different contents of FA under different internal relative humidities. There is no significant variation in chloride ion content at the same depth, especially for the concrete prepared with 15% and 30% FA. However, for the concrete in the environment with a relative humidity of 45%, its chloride ion concentration is increased significantly at the same depth when the replacement of FA reaches 50%. Therefore, there is little effect on porosity and chloride diffusion coefficient when the content of fly ash is less than 30%. In addition, FA is advanced in larger surface area and hollow structure, which provides the reaction sites and increases the absorption capacity of chloride ions. Therefore, considering the strength and chloride diffusion of concrete, the replacement of FA is suggested as less than 30%.

(2) Effect of adding GGBS on chloride transport

Figure 9 shows the chloride ion concentration of concrete with different contents of GGBS under different relative humidities. For F53 concrete under the relative humidity of 45%, its chloride ion concentration is the lowest at the same depth, indicating that the concrete with 50% GGBS admixture has the strongest antichloride capacity. For the concrete under the relative humidity of 45%, 65%, and 80%, respectively, the chloride ion concentration at the same depth is gradually increased, which is higher than that of the concrete without GGBS mixing. Therefore, considering the strength and chloride diffusion of concrete, the replacement of GGBS is suggested as less than 50%.

(3) Effect of compounding FA and GGBS on chloride transport

Figure 10 presents the evolution of chloride ion concentration in concretes under the relative humidity of 65% and different temperatures. The chloride diffusion is inhibited by compounding FA and GGBS, especially under higher temperatures. Meanwhile, the difference in the chloride diffusion coefficient between the normal concrete and that of compounding FA and GGBS is more significant with the increased temperature. The chloride diffusion coefficient of LF50 concrete under the temperature of 65 °C is decreased by about 42.4% less than that of L50 concrete. Therefore, compounding 17% FA and 32% GGBS to replace the OPC is beneficial for improving the antichloride capacity of concrete. Meanwhile, the strength and porosity of concrete is also improved.

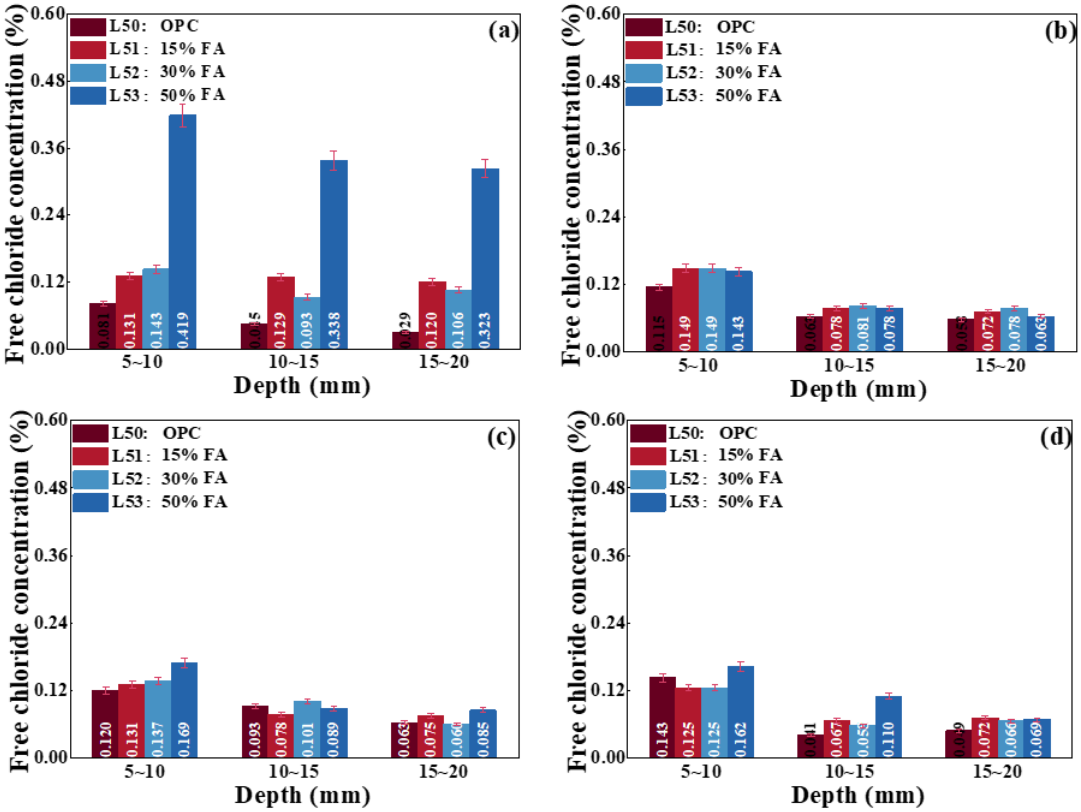

Figure 8. Chloride ion concentration of concrete with different contents of FA under the relative humidity of (**a**) 45%, (**b**) 65%, (**c**) 80%, and (**d**) 100%.

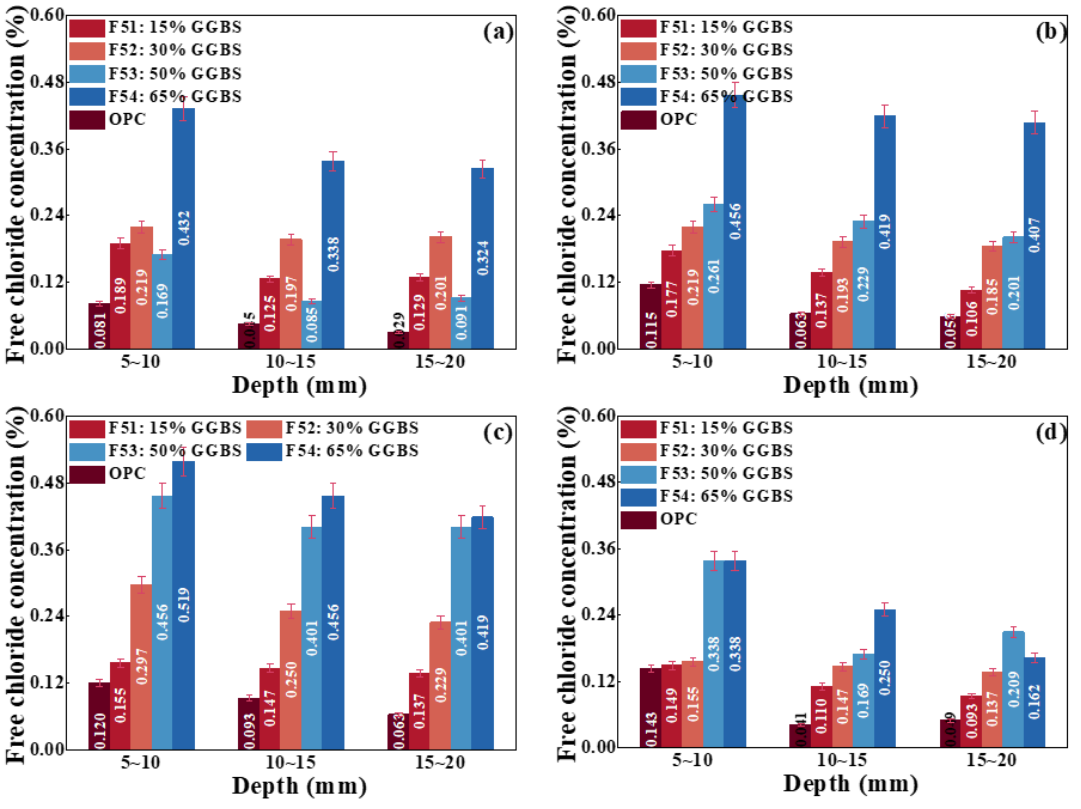

Figure 9. Chloride ion concentration of concrete with different contents of GGBS under the relative humidity of (**a**) 45%, (**b**) 65%, (**c**) 80%, and (**d**) 100%.

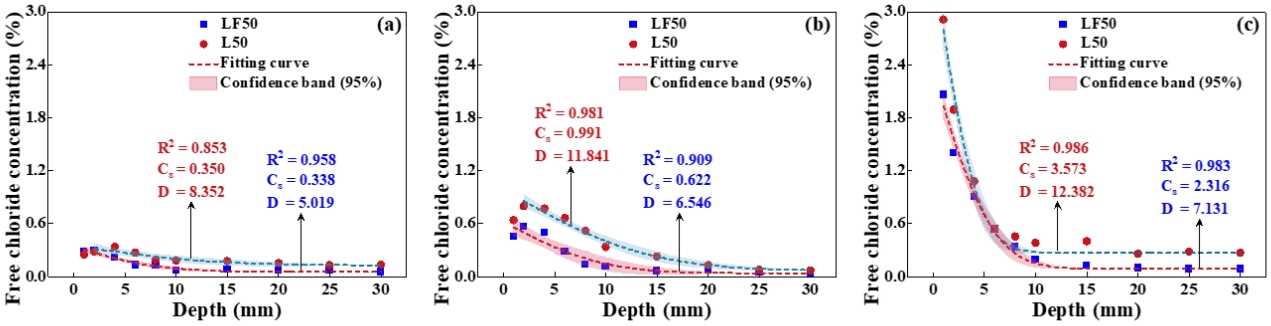

Figure 10. Chloride ion concentration in concretes under the temperatures of (**a**) 25 °C, (**b**) 45 °C, and (**c**) 65 °C.

In summary, temperature, relative humidity, and mineral admixtures will influence the chloride ion transport at the concrete surface. Yet, only individual effects of temperature, relative humidity, and mineral admixtures on the chloride ion transport were analyzed in this paper; also, the conditions of impact factors were limited in this experiment, and a gap with the reality in practical engineering still exists, which may influence the service life prediction of reinforced concrete structures. Moreover, the coupling effects have not been investigated in detail and still need to be deeply studied in the not-distant future.

4.3. Numerical Simulation

4.3.1. Single Effect of Temperature or Relative Humidity on Chloride Transport

(1) Effect of temperature on chloride transport

Based on Equation (4), the single effect of temperature on chloride transport in concrete for 30 d was simulated using the COMSOL software. Figure 11 presents the cloud images of chloride distribution in concrete at the temperatures of 5 °C, 25 °C, 45 °C, and 65 °C. The chloride concentration is decreased with the depth of concrete, and the chloride migrates to greater depths with the increase in temperature. The chloride diffusion depth in concrete is 5 mm, 7.5 mm, 12.5 mm, and 25 mm when the temperature is 5 °C, 25 °C, 45 °C, and 65 °C, respectively. Compared to the experimental result, the effect tendency of temperature on chloride transport obtained with simulation is identical. However, it should be noted that the effect of relative humidity is not considered in Equation (4), inducing an error existing in the diffusion depth. In addition, the chloride enrichment at the ITZ between the aggregate and cement paste is weakened when the temperature reaches 65 °C.

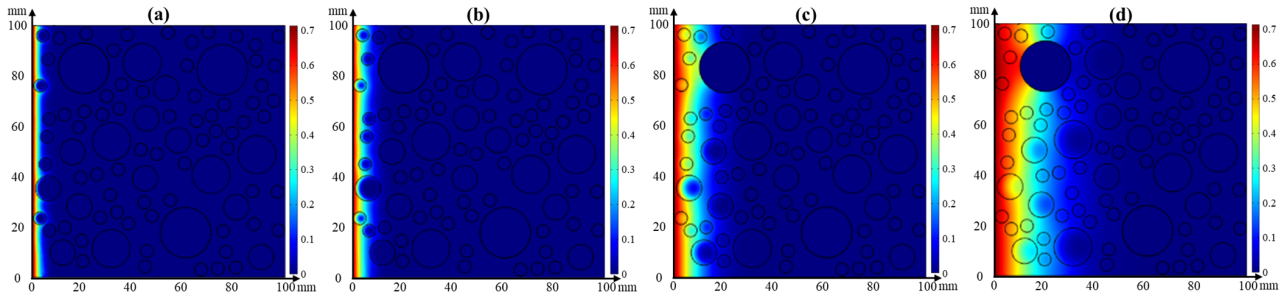

Figure 11. Cloud images of chloride distribution in concrete at the temperature of (**a**) 5 °C, (**b**) 25 °C, (**c**) 45 °C, and (**d**) 65 °C.

(2) Effect of relative humidity on chloride transport

Based on Equation (3), the single effect of relative humidity on chloride transport in concrete for 30 d was simulated using the COMSOL software. Figure 12 presents the cloud images of chloride distribution in concrete at the relative humidity of 45%, 65%, 80%, and 100%. The chloride concentration is decreased with the depth of concrete, and the chloride migrates to greater depths as relative humidity decreases. This effect tendency of

relative humidity on chloride transport is consistent with the experimental result presented in Figure 6. The chloride diffusion depth in concrete is 25 mm, 20 mm, 12.5 mm, and 7.5 mm when the relative humidity is 45%, 65%, 80%, and 100%, respectively. In addition, the chloride is enriched at the ITZ between the aggregate and cement paste, and this phenomenon becomes more pronounced with the decrease in relative humidity. The main reason is that the moisture transport is inhibited by the aggregate, resulting in the decrease in chloride diffusion to the interior of the aggregate.

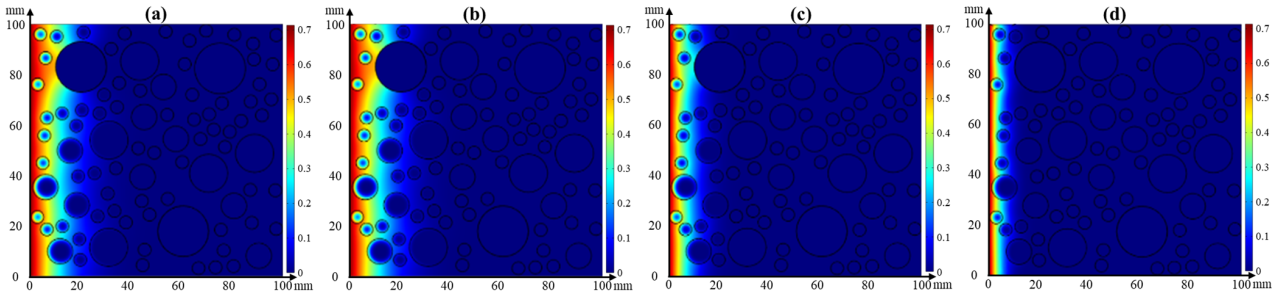

Figure 12. Cloud images of chloride distribution in concrete with a relative humidity of (**a**) 45%, (**b**) 65%, (**c**) 80%, and (**d**) 100%.

4.3.2. Coupled Effect of Temperature and Relative Humidity on Chloride Transport

Based on Equation (5), the coupled effect of temperature and relative humidity on chloride transport in concrete for 30 d was simulated using the COMSOL software. Figure 13 presents the cloud images of chloride distribution in concrete at a constant temperature and relative humidity. The chloride concentration is decreased with the depth of concrete. The effect of temperature on chloride transport in concrete is more significant than that of relative humidity because the chloride migrates to greater depths as the temperature, as shown in Figure 13b. The chloride migrates to the deepest interior of the concrete when the relative humidity is 45% and the temperature is 25 °C. However, there is no significant difference in the chloride transport in concrete at the constant temperature and different relative humidity. It is worth noting that the chloride diffusion capacity of coarse aggregate is improved by the higher temperature while the transport distance is prolonged; furthermore, coarse aggregate has better resistance to chloride penetration than fine aggregates. In addition, the phenomenon of chloride enrichment in the ITZ between the aggregate and cement paste is alleviated.

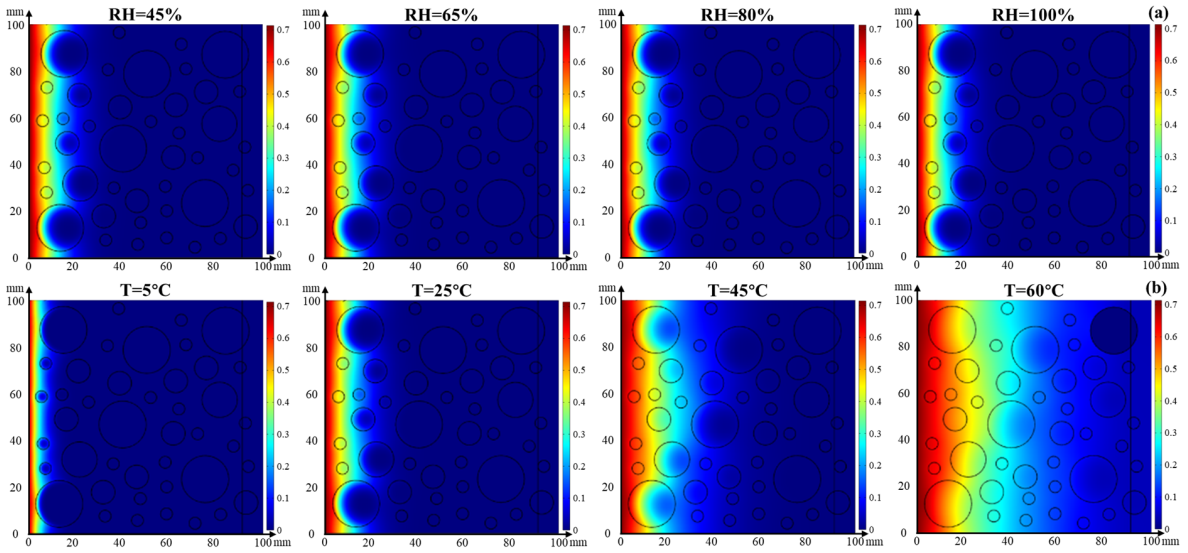

Figure 13. Cloud images of chloride distribution in concrete at (**a**) constant temperature of 25 °C and (**b**) constant relative humidity of 45%.

5. Conclusions

In this work, the coupling effect of temperature, relative humidity, and mineral admixtures (FA and GGBS) on chloride transport in concrete was investigated through experimental and numerical simulation work. The main conclusions are as follows:

1. The replacement of OPC by FA and GGBS is beneficial for improving the strength and capacity of antichloride, and its best dosage is suggested as compounding about 15% FA and 30% GGBS.
2. The chloride diffusion coefficient is decreased with the decreased temperature and growth of relative humidity; however, the chloride concentration on the concrete surface is increased with the growth of temperature and relative humidity. Moreover, the chloride migrates to the deeper interior as the temperature increases.
3. The effect tendency of temperature and relative humidity on chloride distribution in concrete obtained from the numerical simulation is consistent with the experimental result. Moreover, its accuracy is improved when considering the coupled effect of temperature or relative humidity on chloride transport.

Author Contributions: Conceptualization, Z.D.; Methodology, R.Z.; Software, H.X. and R.Z.; Investigation, H.X.; Writing—original draft, Z.D. and S.L.; Writing—review & editing, Z.J. and S.L.; Visualization, Z.D.; Funding acquisition, Z.J. All authors have read and agreed to the published version of the manuscript.

Funding: This work is part of projects financially supported by the National Natural Science Foundation of China (NO. 52078259). Also, this work is financially supported by the Taishan Scholars of Shandong Province (No. ts20190942).

Informed Consent Statement: Informed consent was obtained from all subjects involved in the study.

Data Availability Statement: Data are contained within the article.

Acknowledgments: All the supports are gratefully appreciated.

Conflicts of Interest: Author Huan Xue was employed by the company Qingdao Branch of Beijing Zhongchang Engineering Consulting Co. Ltd. The remaining authors declare that the research was conducted in the absence of any commercial or financial relationships that could be construed as a potential conflict of interest.

References

1. Balestra, C.E.T.; Reichert, T.A.; Savaris, G. Contribution for durability studies based on chloride profiles analysis of real marine structures in different marine aggressive zones. *Constr. Build. Mater.* **2019**, *206*, 140–150. [CrossRef]
2. Lun, P.Y.; Zhang, X.G.; Jiang, C.; Ma, Y.F.; Fu, L. Modelling of Corrosion-Induced Concrete Cover Cracking Due to Chloride Attacking. *Materials* **2021**, *14*, 1440. [CrossRef]
3. Oh, B.H.; Jang, S.Y. Effects of material and environmental parameters on chloride penetration profiles in concrete structures. *Cem. Concr. Res.* **2007**, *37*, 47–53. [CrossRef]
4. Liu, J.; Jiang, Z.L.; Zhao, Y.L.; Zhou, H.; Wang, X.D.; Zhou, H.J.; Xing, F.; Li, S.L.; Zhu, J.H.; Liu, W. Chloride Distribution and Steel Corrosion in a Concrete Bridge after Long-Term Exposure to Natural Marine Environment. *Materials* **2020**, *13*, 3900. [CrossRef] [PubMed]
5. Bui, H.T.; Tan, K.H. Time-dependent nonuniform numerical model of corrosion process and consequent corrosion-induced concrete cracking under chloride attack. *Structures* **2023**, *52*, 332–347. [CrossRef]
6. Petcherdchoo, A. Closed-form solutions for modeling chloride transport in unsaturated concrete under wet-dry cycles of chloride attack. *Constr. Build. Mater.* **2018**, *176*, 638–651. [CrossRef]
7. Ragab, A.M.; Elgammal, M.A.; Hodhod, O.A.; Ahmed, T. Evaluation of field concrete deterioration under real conditions of seawater attack. *Constr. Build. Mater.* **2016**, *119*, 130–144. [CrossRef]
8. Rochanavibhata, U.; Punthutaecha, K.; Petcherdchoo, A. Time-dependent chloride transport models for predicting service life of bridge decks under chloride attack. *Mater. Today Proc.* **2022**, *52*, 2361–2364. [CrossRef]
9. Osio-Norgaard, J.; Gevaudan, J.P.; Srubar, W.V. A review of chloride transport in alkali-activated cement paste, mortar, and concrete. *Constr. Build. Mater.* **2018**, *186*, 191–206. [CrossRef]

10. Homan, L.; Ababneh, A.N.; Xi, Y. The effect of moisture transport on chloride penetration in concrete. *Constr. Build. Mater.* **2016**, *125*, 1189–1195. [CrossRef]
11. Jin, H.; Liu, J.; Zhong, D.; Tang, L. Experimental study on chloride ion diffusion behavior and microstructure in concrete under alternating ambient humidity conditions. *Constr. Build. Mater.* **2023**, *401*, 132886. [CrossRef]
12. Li, S.; Jin, Z.; Chang, H.; Gao, Y. Oxygen diffusion into unsaturated seawater and sea sand concrete and its effect on non-uniform corrosion of steel bars. *J. Build. Eng.* **2024**, *84*, 108665. [CrossRef]
13. Ortolan, T.L.P.; Borges, P.M.; Silvestro, L.; Da Silva, S.R.; Possan, E.; Andrade, J.J.O. Durability of concrete incorporating recycled coarse aggregates: Carbonation and service life prediction under chloride-induced corrosion. *Constr. Build. Mater.* **2023**, *404*, 133267. [CrossRef]
14. Li, S.; Jin, Z.; Pang, B.; Li, J. Durability performance of an RC beam under real marine all corrosion zones exposure for 7 years. *Case Stud. Constr. Mater.* **2022**, *17*, e01516. [CrossRef]
15. Gašpárek, J.; Húlek, L.; Paulík, P.; Janotka, I. Theoretical prediction of chloride diffusion into concrete compared to natural chloride contamination of existing bridges. *Structures* **2023**, *57*, 105080. [CrossRef]
16. Reichert, T.A.; Balestra, C.E.T.; Medeiros-Junior, R.A.D. Coupled model on the variation of diffusion coefficient and surface chloride concentration in reinforced concrete structures over time. *Constr. Build. Mater.* **2024**, *411*, 134715. [CrossRef]
17. Homayoonmehr, R.; Rahai, A.; Ramezanianpour, A.A. Predicting the chloride diffusion coefficient and surface electrical resistivity of concrete using statistical regression-based models and its application in chloride-induced corrosion service life prediction of RC structures. *Constr. Build. Mater.* **2022**, *357*, 129351. [CrossRef]
18. Jin, H.; Fan, X.; Li, Z.; Zhang, W.; Liu, J.; Zhong, D.; Tang, L. An experimental study on the influence of continuous ambient humidity conditions on relative humidity changes, chloride diffusion and microstructure in concrete. *J. Build. Eng.* **2022**, *59*, 105112. [CrossRef]
19. Wu, L.; Gao, X.; Xia, Y. Randomness and time-varying characteristics of chloride ion transport in existing harbor concrete structures. *Constr. Build. Mater.* **2024**, *412*, 134839. [CrossRef]
20. Yu, Z.; Chen, Y.; Liu, P.; Wang, W. Accelerated simulation of chloride ingress into concrete under drying–wetting alternation condition chloride environment. *Constr. Build. Mater.* **2015**, *93*, 205–213. [CrossRef]
21. Wang, Y.; Guo, S.; Yan, B.; Liu, Z.; Wang, Y.; Yuan, C. Experimental and analytical investigation on chloride ions transport in concrete considering the effect of dry-exposure ratio under diurnal tidal environment. *Constr. Build. Mater.* **2022**, *328*, 127138. [CrossRef]
22. Al-Sodani, K.A.A.; Al-Zahrani, M.M.; Maslehuddin, M.; Al-Amoudi, O.S.B.; Al-Dulaijan, S.U. Chloride diffusion models for plain and blended cement concretes exposed to laboratory and atmospheric marine conditions. *J. Mater. Res. Technol.* **2022**, *17*, 125–138. [CrossRef]
23. Pansera, W.A.; Reichert, T.A.; Savaris, G.; Balestra, C.E.T. Nonlinear regression using Gaussian-Lorentzian functions to empirical modeling of convective-diffusive chloride transport in concrete. *Constr. Build. Mater.* **2022**, *341*, 127770. [CrossRef]
24. Korec, E.; Jirásek, M.; Wong, H.S.; Martínez-Pañeda, E. Phase-field chemo-mechanical modelling of corrosion-induced cracking in reinforced concrete subjected to non-uniform chloride-induced corrosion. *Theor. Appl. Fract. Mech.* **2024**, *129*, 104233. [CrossRef]
25. Sun, C.; Yuan, L.; Zhai, X.; Qu, F.; Li, Y.; Hou, B. Numerical and experimental study of moisture and chloride transport in unsaturated concrete. *Constr. Build. Mater.* **2018**, *189*, 1067–1075. [CrossRef]
26. Dehwah, O.H.A.; Xi, Y. Theoretical model for the coupling effect of moisture transport on chloride penetration in concrete. *Cem. Concr. Res.* **2024**, *177*, 107431. [CrossRef]
27. Lian, S.; Meng, T.; Zhao, Y.; Liu, Z.; Zhou, X.; Ruan, S. Experimental and theoretical analyses of chloride transport in recycled concrete subjected to a cyclic drying-wetting environment. *Structures* **2023**, *52*, 1020–1034. [CrossRef]
28. Liu, Q.-F.; Cai, Y.; Peng, H.; Meng, Z.; Mundra, S.; Castel, A. A numerical study on chloride transport in alkali-activated fly ash/slag concretes. *Cem. Concr. Res.* **2023**, *166*, 107094. [CrossRef]
29. Lee, J.M.; Hong, S.I.; Yang, H.J.; Jung, D.H. Numerical Modeling of Chloride Transport in Concrete under Cyclic Exposure to Chloride. *Materials* **2022**, *15*, 5966. [CrossRef]
30. Jain, A.; Gencturk, B. Multiphysics and Multiscale Modeling of Coupled Transport of Chloride Ions in Concrete. *Materials* **2021**, *14*, 885. [CrossRef]
31. Liu, Z.; Wang, Y.; Wang, J.; Liu, C.; Jiang, J.; Li, H. Experiment and simulation of chloride ion transport and binding in concrete under the coupling of diffusion and convection. *J. Build. Eng.* **2022**, *45*, 103610. [CrossRef]
32. Vieira, D.R.; Moreira, A.L.R.; Calmon, J.L.; Dominicini, W.K. Service life modeling of a bridge in a tropical marine environment for durable design. *Constr. Build. Mater.* **2018**, *163*, 315–325. [CrossRef]
33. da Costa, A.; Fenaux, M.; Fernández, J.; Sánchez, E.; Moragues, A. Modelling of chloride penetration into non-saturated concrete: Case study application for real marine offshore structures. *Constr. Build. Mater.* **2013**, *43*, 217–224. [CrossRef]
34. Violetta, B.K. Life-365 Service Life Prediction Model. *Concr. Int.* **2002**, *24*, 53–57.
35. Xi, Y.; Zdeněk, P.B. Modeling Chloride Penetration in Saturated Concrete. *J. Mater. Civ. Eng.* **1999**, *11*, 58–65. [CrossRef]
36. Ababneh, A.; Benboudjema, F.; Xi, Y. Chloride Penetration in Nonsaturated Concrete. *J. Mater. Civ. Eng.* **2003**, *15*, 183–191. [CrossRef]

37. Chen, D.; Guo, W.; Wu, B.; Ye, T. Mesoscopic characteristics and spatiotemporal variability of chloride transport in concrete. *Constr. Build. Mater.* **2024**, *415*, 135081. [CrossRef]
38. Kang, X.; Tong, X.-Y.; Chen, R.-P.; Chen, Y.-Q. Effect of ITZ on chloride ion transport in recycled aggregate concrete: Analytical and numerical studies. *J. Build. Eng.* **2024**, *83*, 108443. [CrossRef]

Disclaimer/Publisher's Note: The statements, opinions and data contained in all publications are solely those of the individual author(s) and contributor(s) and not of MDPI and/or the editor(s). MDPI and/or the editor(s) disclaim responsibility for any injury to people or property resulting from any ideas, methods, instructions or products referred to in the content.